

This is an Open Access document downloaded from ORCA, Cardiff University's institutional repository: <https://orca.cardiff.ac.uk/id/eprint/114134/>

This is the author's version of a work that was submitted to / accepted for publication.

Citation for final published version:

Ujiie, Kohtaro, Saishu, Hanae, Fagereng, Åke, Nishiyama, Naoki, Otsubo, Makoto, Masuyama, Haruna and Kagi, Hiroyuki 2018. An explanation of episodic tremor and slow slip constrained by crack-seal veins and viscous shear in subduction mélange. *Geophysical Research Letters* 45 (11), pp. 5371-5379. 10.1029/2018GL078374

Publishers page: <http://dx.doi.org/10.1029/2018GL078374>

Please note:

Changes made as a result of publishing processes such as copy-editing, formatting and page numbers may not be reflected in this version. For the definitive version of this publication, please refer to the published source. You are advised to consult the publisher's version if you wish to cite this paper.

This version is being made available in accordance with publisher policies. See <http://orca.cf.ac.uk/policies.html> for usage policies. Copyright and moral rights for publications made available in ORCA are retained by the copyright holders.



An explanation of episodic tremor and slow slip constrained by crack-seal veins and viscous shear in subduction mélange

Kohtaro Ujiie^{1,2*}, Hanae Saishu^{3,4}, Åke Fagereng⁵, Naoki Nishiyama¹, Makoto Otsubo⁴, Haruna Masuyama¹, and Hiroyuki Kagi⁶

¹ Graduate School of Life and Environmental Sciences, University of Tsukuba, Japan.

² Research and Development Center for Ocean Drilling Science, Japan Agency for Marine-Earth Science and Technology, Japan.

³ Renewable Energy Research Center, National Institute of Advanced Industrial Science and Technology, Japan.

⁴ Geological Survey of Japan, National Institute of Advanced Industrial Science and Technology, Japan.

⁵ School of Earth and Ocean Sciences, Cardiff University, UK.

⁶ Geochemical Research Center, Graduate School of Science, The University of Tokyo, Japan.

*Corresponding author: Kohtaro Ujiie (kujiie@geol.tsukuba.ac.jp)

Key Points:

- Crack-seal veins in subduction mélange record repeated low-angle thrust faulting under tensile overpressure
- The minimum time interval between thrusting events is comparable to recurrence intervals of slow earthquakes
- Crack-seal veins and viscous shear zones in subduction mélange may be geological manifestations of episodic tremor and slow slip

27 **Abstract**

28 Episodic tremor and slow slip (ETS) occurs in the transition zone between the
 29 locked seismogenic zone and the deeper, stably sliding zone. Actual mechanisms of ETS
 30 are enigmatic, caused by lack of geological observations and limited spatial resolution of
 31 geophysical information from the ETS source. We report that quartz-filled, crack-seal
 32 shear and extension veins in subduction mélangé record repeated low-angle thrust-sense
 33 frictional sliding and tensile fracturing at near-lithostatic fluid pressures. Crack-seal veins
 34 were coeval with viscous shear zones that accommodated deformation by pressure
 35 solution creep. The minimum time interval between thrusting events, determined from a
 36 kinetic model of quartz precipitation in shear veins, was less than a few years. This short
 37 recurrence time of low-angle brittle thrusting at near-lithostatic fluid overpressures
 38 within viscous shear zones may be explained by frequent release of accumulated strain by
 39 ETS.

40

41 **1. Introduction**

42 A spectrum of slow earthquake behaviors, including low-frequency tectonic tremors
 43 (LFTs), low-frequency earthquakes (LFEs), very-low-frequency earthquakes (VLFs),
 44 and slow slip events (SSEs), has been detected from seismologic and geodetic
 45 observations [*Schwartz and Rokosky, 2007; Peng and Gomberg, 2010; Beroza and Ide,*
 46 *2011; Saffer and Wallace, 2015; Obara and Kato, 2016*]. Tectonic tremor is defined as a
 47 persistent low frequency seismic signal that lasts for days to weeks but is interpreted to

represent a swarm of LFEs that accommodate shear slip on low-angle thrusts [*Shelly et al.*, 2007; *Ide et al.*, 2007]. Slow slip is a geodetically detected, transient creep event where slip speed exceeds average plate motion but is too slow to generate detectable seismic waves. On some faults, slow slip events appear to repeat near-periodically in the same location, and in some places these events are spatiotemporally accompanied by LFTs, referred to as episodic tremor and slow slip (ETS) [*Rogers and Dragert*, 2003; *Obara et al.*, 2004].

In subduction zones, slow earthquake phenomena generally occur in transition zones between interseismically locked and stably sliding fault segments [*Schwartz and Rokosky*, 2007; *Peng and Gombert*, 2010]. ETS events are typically observed along the plate boundary thrust near the mantle wedge corner in relatively warm subduction zones. These events repeat at least every few years, and thus lead to episodic transfer of stress from the ETS region to the locked seismogenic zone; this stress change may contribute to trigger megathrust earthquakes [*Obara and Kato*, 2016]. Recent studies in the Nankai subduction zone have revealed that LFTs, LFEs, and SSEs occur along the plate boundary at depths of ~6–9 km and ~15 km [*Yamashita et al.*, 2015; *Araki et al.*, 2017; *Nakano et al.*, 2018]. The components of ETS can therefore be generated along the plate boundary at depths much shallower than the mantle wedge corner.

Despite the importance for understanding the dynamics of slow earthquakes and their relation to megathrust earthquakes, the underlying deformation mechanisms responsible for slow earthquake-generated deformation remain poorly understood. This shortfall in physical understanding arises from insufficient geological information on

slow earthquakes, limited constraint on the temporal relationship between slow earthquakes and ordinary megathrust earthquakes, and poor spatial constraints on the source area of slow earthquakes and the spatiotemporal relation between tremor and slow slip. Whereas geological evidence for high-speed slip, such as pseudotachylyte (solidified frictional melt produced by seismic slip), has been reported from subduction zones [Ujiie *et al.*, 2007; Ujiie and Kimura, 2014], low-speed deformation responsible for slow earthquakes have been attributed to brittle failure of relatively strong lenses coincident with viscous shear in surrounding matrix [Skarbek *et al.*, 2012; Fagereng *et al.*, 2014; Hayman and Lavier, 2014; Behr *et al.*, 2018].

The exhumed Makimine mélange in the Late Cretaceous Shimanto accretionary complex of eastern Kyushu, southwest Japan (Figure 1) records progressive plate boundary deformation during subduction of young, warm oceanic crust to a shallow (10–15 km) frictional-viscous transition where temperatures reached 300–350 °C [Mackenzie *et al.*, 1987; Hara and Kimura, 2008; Palazzin *et al.*, 2016]. This mélange is exhumed from a frictional-viscous transition zone, typical of where slow earthquakes commonly occur. We examine the potential record of slow earthquakes by considering four key geophysical observations from active subduction margins [Rogers and Dragert, 2003; Obara *et al.*, 2004; Schwartz and Rokosky, 2007; Peng and Gomberg, 2010; Beroza and Ide, 2011; Saffer and Wallace, 2015; Obara and Kato, 2016; Wallace *et al.*, 2016; Araki *et al.*, 2017]: (1) slow earthquakes typically occur in regions of high fluid pressure and low effective stress; (2) VLFs, and triggered swarms of LFs associated with SSEs, have very low stress drops (tens of kilopascal) implying that the effective

fault strength is very weak and sensitive to perturbations; (3) when the focal mechanism is determined, slow earthquakes commonly exhibit shear slip on low-angle thrust faults subparallel to the plate boundary interface; and (4) ETS events repeat every several months to a few years.

2. Geological setting

The Shimanto accretionary complex distributed along the Pacific side of southwest Japan has been believed to represent an ancient on-land analog of the Nankai Trough subduction zone (Figure 1a) [Ujiie and Kimura, 2014]. The Makimine mélange in the Shimanto accretionary complex of eastern Kyushu is Cenomanian to Campanian/Maastrichtian in age (Late Cretaceous) and experienced prehnite-actinolite to greenschist facies metamorphism at 10–15 km depth [Hara and Kimura, 2008; Palazzin *et al.*, 2016]. The maximum temperatures determined from Raman spectra of carbonaceous material, vitrinite reflectance, and illite crystallinity range from 300 to 350 °C [Hara and Kimura, 2008; Palazzin *et al.*, 2016; supporting information]. The mélange generally dips north-northwestward. The Makimine mélange preserves ocean plate stratigraphy composed, in ascending order, of (1) mudstone-dominated mélange containing basalt lenses and hemipelagic red mudstone at the base, (2) reddish brown tuff, and (3) sandstone-mudstone mélange and coherent turbidites (Figure 1b). This stratigraphy is repeated at least twice along the coastal exposure, possibly caused by duplex underplating after subduction, with the apparent thickness of each thrust sheet in the range 1300–1600 m. The subduction-related deformation at the frictional-viscous

transition is well preserved [Mackenzie *et al.*, 1987; Palazzin *et al.*, 2016]. Stretching lineations defined by aligned mica prisms, quartz rods, and long axes of sandstone blocks are particularly well developed in the structurally lower part of the *mélange* (Figure 1c). This lineation represents constrictional strain and is interpreted as parallel to the tectonic transport direction during subduction-related deformation, and indicates that the subduction direction was perpendicular to the general strike of the *mélange* (Figure 1d).

3. Crack-seal veins and viscous shear zones in subduction *mélange*

A 10–60 m thick zone where quartz veins are highly concentrated occurs in the lower part of the Makimine *mélange*, within which a penetrative foliation is defined by pressure solution cleavage (Figure 1b). Along-strike continuity and across-strike structural repetition of the vein concentration zone, and no spatial correlation between the vein distribution zone and the thrust accommodating underplating, indicate that the zone of vein concentration was formed during subduction and prior to the underplating that incorporated the *mélange* into the overlying accretionary prism (Figure 1b). Shear veins, foliation-parallel extension veins, subvertical extension veins, and viscous shear zones are recognized within the vein concentration zone (Figure 2).

Shear veins are subparallel to the *mélange* foliation, with along-strike length ranging from 1 to 10 m (typically about 1 m) (Figures 2a and 3a). Shear veins are laminated and fibrous (Figure 2b), representing multiple episodes of dilation and quartz precipitation along shear surfaces. The internal texture of shear veins is characterized by crack-seal

texture defined by phyllosilicate inclusion bands subparallel to vein margins, with spacing ranging from 20 to 38 μm (Figure 2c and supporting information). At dilational stepovers, the inclusion bands are oblique to vein margins, and slip increments determined from fiber growth increments are 0.1–0.2 mm (Figure 2d). On the basis of the dip direction of inclusion bands at dilational stepovers and steps on the vein surfaces, shear veins exhibit thrust shear sense (Figures 2b and 2d). Slickenfiber orientations are consistent with the top-SSE shear direction determined from the trend of stretching lineations (Figures 1d and 3a). Tectonic reconstructions indicate subduction towards the NNW [Whittaker *et al.*, 2007; Müller *et al.*, 2008], consistent with top-SSE shear, and thus the kinematics of both stretching lineations and localized, frictional shear veins are compatible with low-angle thrust faulting during subduction.

Foliation-parallel extension veins also show crack-seal texture marked by development of inclusion bands of ~28–42 μm spacing but lack dilational stepovers and slickenfibers on vein surfaces (Figure 2a). The length of foliation-parallel extension veins along strike is typically ~1 m, similar to that of shear veins. Subvertical extension veins are straight or sigmoidal, commonly constituting localized *en echelon* arrays (Figure 2e). Quartz crystals within the subvertical veins are elongate with long axes perpendicular to vein margins (Figure 2f), and a crack-seal texture is defined by 25 μm spaced inclusion bands aligned parallel to vein boundaries. Viscous shear zones are defined by < 10 m thick zones of rotated *mélange* foliations (Figure 2g). The viscous deformation is accommodated by pressure solution creep, illustrated by dark selvages and precipitates in pressure shadows, and commonly shows thrust shear sense. Some

shear veins, subhorizontal extension veins, and subvertical extension veins cut the asymmetric fabric formed by viscous shear (Figure 2h), but are also themselves viscously deformed (Figure 2g). These features indicate that brittle shear slip with tensile fracturing and viscous shear occurred contemporaneously.

4. Low-angle thrust faulting under tensile overpressure

Pressure solution cleavage forms perpendicular to the greatest principal compressive stress (σ_I) and thus the low-angle foliation implies a subvertical σ_I , consistent with subvertical extension veins. However, this foliation reflects finite strain and may therefore reflect long-term subvertical shortening, rather than stresses driving fracturing [e.g. *Fisher and Byrne*, 1987; *Ujiie*, 2002; *Fagereng*, 2013]. It is conceivable that σ_I was consistently subvertical and foliation-parallel extension veins involved opening of low cohesion, weak planes. However, this interpretation becomes problematic, because (1) it requires σ_I to become tensile, and (2) it is difficult to explain the gentle dip of crack-seal bands within shear veins and foliation-parallel extension veins. We therefore suggest that the stress repeatedly rotated, which resulted in subvertical extension veins and foliation-parallel extension veins formed in different stress fields. As pointed out by *Meneghini and Moore* [2007], both explanations above require cyclicity in effective normal stress.

A very small angle ($\sim 5.5^\circ$) between the average orientations of shear veins and foliation-parallel extension veins indicates that shear veins were formed as hybrid extensional-shear fractures under low differential stress of $4T_0 < \Delta\sigma < 5.66T_0$ [*Secor*,

1965], where T_0 is the rock tensile strength, and $\Delta\sigma$ is the differential stress (Figures 3a–3c). This is consistent with that shear veins opened at a high angle to the vein margin (Figure 2c). The geometrical relation between shear veins and foliation-parallel extension veins may represent fault-fracture meshes developed in a compressional regime [Sibson, 2017], where thrust faults lie at very low angles to σ_I , and the least principal compressive stress (σ_3) is approximately equal to the vertical stress (σ_V) (Figure 3d). Under such a compressional regime, shear veins and hydraulic extension veins are expected to develop at near-lithostatic and supralithostatic fluid overpressures, respectively, as a result of opening directions of subhorizontal tensile veins being subparallel to the subvertical σ_3 . Supposing $T_0 = 1$ MPa, a low estimate for typical pelitic rocks [Lockner, 1995] to account for the deformed nature of *mélange* mudstones, shear strength (τ) at a very low angle to σ_I (5.5°) is extremely low, $0.38 < \tau < 0.54$ MPa. In this model, the mutually crosscutting relationship between the shear veins and local arrays of subvertical tensile veins, as well as the presence of stylolites and folded phyllosilicate inclusion bands in shear veins (Figure 2d), imply that the local stress field could transiently swap between vertical σ_3 and vertical σ_I , which is also indicative of low differential stress. If, like Fagereng *et al.* [2011], we assume a low shear modulus of 3 GPa for the *mélange* rocks, the stress drop for 0.1–0.2 mm slip increments on 1–10 m long faults is 30–600 kPa, consistent with very low driving stresses.

The observations and model presented here differ in geometry from that described by Fagereng *et al.* [2011]. The vein system they describe, in the Chrystalls Beach Complex, New Zealand, consistently shows coeval shear and extension veins

formed under a subvertical σ_l . The steep σ_l determined in the Chrystalls Beach Complex is typical of weak, underthrust sediments [e.g. *Fisher and Byrne*, 1987], consistent also with thrust faults there developed along weak, low cohesion, clay-rich cleavage [*Fagereng et al.*, 2010]. In the Makimine mélange, a horizontal σ_l explains many of the brittle structures, but episodically the stress field switched to vertical σ_l . This may be a dynamic effect, as also seen in focal mechanisms before and after the 2011 Tohoku-Oki earthquake [e.g., *Hasegawa et al.*, 2011; *Lin et al.*, 2013]. Why the dominant stress field differs between Chrystalls Beach mélange and Makimine mélange shear veins is unclear, but may relate to differences in the frictional strength of the fault surfaces or the bulk rheology of the mélanges. In both cases, however, thrust sense faulting occurred episodically at low differential stress and near-lithostatic fluid pressure.

5. Time interval between crack-seal events

The crack-seal textures in shear and extension veins indicate that discontinuous deformation occurred repeatedly and we interpret the repetition to correlate with temporal fluid pressure variations. To investigate the time required between each crack-seal event, a kinetic model for quartz precipitation [*Rimstidt and Barnes*, 1980], driven by movement of fluid down a pressure gradient, was applied for quartz-filled shear veins (supporting information). The model considers the width of inclusion bands in shear veins (20–38 μm), the typical length of shear veins (1 m), fluid pressure reduction at the start of each crack-seal event, and ambient temperature of 300–330 °C

(supporting information). Assuming that subhorizontal tensile fractures require at least lithostatic fluid pressures, and that opening of these fractures creates at least temporarily an interconnected fluid pathway, we consider a local fluid pressure change equal to lithostatic minus hydrostatic pressure at the time of fracture opening. At 10–15 km depth with average rock density of 2600 kg/m^3 , this is a fluid pressure drop of 157–235 MPa. This large fluid pressure drop is consistent with various vapor/liquid ratios in two-phase fluid inclusions within shear veins (supporting information). Assuming precipitation rate controls the time of healing (i.e. silica can be transported to the open fracture at least as far as quartz precipitates), the veins can close in less than 1.6–4.5 years (Figure 4). Quartz crystals are blocky and do not show collapse structures, which is consistent with precipitation in an open crack that did not collapse. This lack of collapse structures may be surprising upon a large fluid pressure drop, but could possibly be explained by relatively fast precipitation from fluids moving through the fracture system in response to increased fracture permeability [cf. *Vrolijk*, 1987]. On the other hand, we note that the large fluid pressure drop may have limited crack propagation and locally arrested shear displacement. We thus assume this $\leq 1.6\text{--}4.5$ years estimate corresponds to minimum healing time between deformation events. If the fluid temperature is higher than ambient temperature, the model suggests that healing time becomes shorter, and similarly, if precipitation is coupled to collapse of pore space under increasing effective normal stress, healing rates will also increase [*Rimstidt and Barnes*, 1980].

6. Discussion and Conclusion

Our results show that shear veins in subduction mélangé record low-angle thrust faulting at very small shear strength and near-lithostatic fluid overpressures, consistent with plate boundary shear kinematics and key geophysical observations of slow earthquakes in subduction zones. The time required between discrete vein opening events, assuming complete healing of cracks defined by inclusion band spacing, gives a constraint of $\leq 1.6\text{--}4.5$ years for the minimum time interval of repeated thrust faulting events. This repeat time is comparable to recurrence intervals of slow earthquakes. A large number ($\sim 100\text{--}150$) of inclusion bands in shear veins (supporting information) indicate multiple occurrences of fracturing under elevated fluid pressure and subsequent restoration of cohesive and tensile strength through hydrothermal precipitation. If the slip increment of $\sim 0.1\text{--}0.2$ mm at dilational stepovers correspond to the shear displacement during a single slow earthquake, $\sim 100\text{--}150$ inclusion bands suggest that cumulative displacement along individual low-angle thrust faults is $\sim 0.01\text{--}0.03$ m. Alternatively, the total displacement during a single slow earthquake event may be distributed into many different shear surfaces. In this case, the slip increment of $\sim 0.1\text{--}0.2$ mm during one crack-seal event could accommodate a small component of the total displacement during that slow earthquake. Crack-seal shear and extension veins are also recognized in other mélanges and metamorphic rocks exhumed from the source depths of slow earthquakes [Fagereng *et al.*, 2011; Fisher and Brantley, 2014; Sibson, 2017]. Such crack-seal veins may also record repeated slow earthquake events.

In the Makimine mélange, the intensely veined zone is tens of meters thick, and involves a combination of viscous and frictional deformation. Such frictional-viscous deformation zones that are narrower than the full width of a mélange shear zone have been reported from other exhumed subduction zones, irrespective of deformation mechanisms of pressure solution creep or dislocation creep [Rowe *et al.*, 2013; Fagereng *et al.*, 2014]. Within a mélange shear zone, frictional-viscous deformation along narrow zones could represent deformation at higher strain rates. The absence of geological evidence of frictional heat (e.g. pseudotachylytes) in narrow shear zones suggests that strain rate is slower than seismic slip rate. Therefore, if localization of viscous shear into narrow zones implies higher strain rates [cf. Fagereng *et al.*, 2014], then these may be candidates for slow earthquake zones. A common feature is coexistence of mineralized veins and relatively intense viscous fabrics, implying locally elevated fluid pressures and increased viscous strains, respectively. The geophysically observed signature of such deformation may be transient slow slip faster than plate motion rates (SSEs) accompanied by localized frictional failure (tremor containing LFEs).

Acknowledgements. This work is supported by Japan Society for the Promotion of Science KAKENHI grant JP16H06476. A.F. is supported by ERC Starting Grant 715836 “MICA”. Structural, Raman, and fluid inclusion data, and parameters and values used in the kinetic modeling are available in the supplementary materials. J. Kirkpatrick and an anonymous reviewer provided valuable comments that significantly improved the manuscript. We thank GRL Editor Lucy Flesch for evaluation of the paper.

We would also like to thank K. Ohta, Y. Yamashita, S. Katakami, and Y. Ito for valuable discussions.

References

- Akinfiyev, N. N., and L. W. Diamond (2009), A simple predictive model of quartz solubility in water-salt-CO₂ systems at temperatures up to 1000 °C and pressures up to 1000 MPa, *Geochim. Cosmochim. Acta*, *73*, 1597–1608.
- Araki, E., et al. (2017), Recurring and triggered slow-slip events near the trench at the Nankai Trough subduction megathrust, *Science*, *356*, 1157–1160.
- Behr, W. M., A. J. Kotowski, and K. T. Ashley (2018), Dehydration-induced rheological heterogeneity and the deep tremor source in warm subduction zones, *Geology*, *46*, <https://doi.org/10.1130/G40105.1>.
- Beroza, G. C., and S. Ide (2011), Slow earthquakes and nonvolcanic tremor, *Annu. Rev. Earth Planet. Sci.*, *39*, 271–296.
- Fagereng, A. (2013), On stress and strain in a continuous-discontinuous shear zone undergoing simple shear and volume loss, *J. Struct. Geol.*, *50*, 44–53.
- Fagereng, A., F. Remitti, R. H. Sibson (2010), Shear veins observed within anisotropic fabric at high angles to the maximum compressive stress, *Nat. Geosci.*, *3*, 482–485.
- Fagereng, A., F. Remitti, R. H. Sibson (2011), Incrementally developed slickenfibres—Geological record of repeating low stress-drop seismic events, *Tectonophysics*, *510*, 381–386.

- 310 Fagereng, A., G. W. B. Hillary, J. F. A. Diener (2014), Brittle-viscous deformation, slow slip,
 311 and tremor, *Geophys. Res. Lett.*, *41*, 4159–4167.
- 312 Fisher, D., and T. Byrne (1987), Structural evolution of underthrust sediments, Kodiak
 313 Island, Alaska, *Tectonics*, *6*, 775–793.
- 314 Fisher, D. M., and S. L. Brantley (2014), The role of silica redistribution in the evolution of
 315 slip instabilities along subduction interfaces: Constraints from the Kodiak accretionary
 316 complex, Alaska, *J. Struct. Geol.*, *69*, 395–414.
- 317 Hara, H., and K. Kimura (2008), Metamorphic and cooling history of the Shimanto
 318 accretionary complex, Kyushu, Southwest Japan: Implications for the timing of
 319 out-of-sequence thrusting, *Isl. Arc*, *17*, 546–559.
- 320 Hasegawa, A., K. Yoshida, and T. Okada (2011), Nearly complete stress drop in the 2011 M_w
 321 9.0 off the Pacific coast of Tohoku earthquake, *Earth Planets Space*, *69*, 703–707.
- 322 Hayman, N. W., and L. L. Lavier (2014), The geological record of deep episodic tremor and
 323 slip, *Geology*, *42*, 195–198.
- 324 Ide, S., D. R. Shelly, and G. C. Beroza (2007), Mechanism of deep low frequency
 325 earthquakes: Further evidence that deep non-volcanic tremor is generated by shear slip
 326 on the plate interface, *Geophys. Res. Lett.*, *34*, L03308.
- 327 Kagi, H. et al. (1994), Proper understanding of down-shifted Raman spectra of natural
 328 graphite: Direct estimation of laser-induced rise in sample temperature, *Geochim.*
 329 *Cosmochim. Acta*, *58*, 3527–3530.
- 330 Kouketsu, Y. et al. (2014), A new approach to develop the Raman carbonaceous material
 331 geothermometer for low-grade metamorphism using peak width, *Isl. Arc*, *23*, 33–50.

- 332 Lahfid, A. et al. (2010), Evolution of the Raman spectrum of carbonaceous material in
 333 low-grade metasediments of the Glarus Alps (Switzerland), *Terra Nova*, 22, 354–360.
- 334 Lin, W., et al. (2013), Stress state in the largest displacement area of the 2011 Tohoku-Oki
 335 earthquake, *Science*, 339, 687–690.
- 336 Lockner, D. A. *Rock Physics and Phase Relations, A Handbook of Physical Constants*, 127–
 337 147 (AGU, 1995).
- 338 Mackenzie, J. S., D. T. Needham, and S. M. Agar (1987), Progressive deformation in an
 339 accretionary complex: An example from the Shimanto belt of eastern Kyushu,
 340 southwest Japan, *Geology*, 15, 353–356.
- 341 Meneghini, F. and J. C. Moore (2007), Deformation and hydrofracture in a subduction thrust
 342 at seismogenic depths: The Rodeo Cove thrust zone, Marin Headlands, California, *GSA*
 343 *Bulletin*, 119, 174–183.
- 344 Müller, R. D., et al. (2008), Long-term sea-level fluctuations driven by ocean basin dynamics,
 345 *Science*, 319, 1357–1362.
- 346 Nakano, M., T. Hori, E. Araki, S. Kodaira, and S. Ide (2018), Shallow very-low-frequency
 347 earthquakes accompany slow slip events in the Nankai subduction zone, *Nat. Commun.*,
 348 984, doi:10.1038/s41467-018-03431-5.
- 349 Obara, K., and A. Kato (2016), Connecting slow earthquakes to huge earthquakes, *Science*,
 350 353, 253–257.
- 351 Obara, K., H. Hirose, F. Yamamizu, and K. Kasahara (2004), Episodic slow slip events
 352 accompanied by non-volcanic tremors in southwest Japan subduction zone, *Geophys.*
 353 *Res. Lett.*, 31, L23602.

- 354 Okamoto, A. and K. Sekine (2011), Textures of syntaxial quartz veins synthesized by
355 hydrothermal experiments, *J. Struct. Geol.*, *33*, 1764–1775.
- 356 Okamoto, A., H. Saishu, N. Hirano, and N. Tsuchiya (2010), Mineralogical and textural
357 variation of silica minerals in htdrothermal flow-through experiments: Implications for
358 quartz vein formationm *Geochim. Cosmochim. Acta*, *74*, 3692–3706.
- 359 Palazzin, G., et al. (2016), Deformation processes at the down-dip limit of the seismogenic
360 zone: The example of Shimanto accretionary complex, *Tectonophysics*, *687*, 28–43.
- 361 Peng, Z., and J. Gomberg (2010), An integrated perspective of the continuum between
362 earthquakes and slow slip phenomena, *Nat. Geosci.*, *3*, 599–607.
- 363 Rimstidt, J. D., and H. L. Barnes (1980), The kinetics of silica-water reactions, *Geochim.*
364 *Cosmochim. Acta*, *44*, 1683–1699.
- 365 Rogers, G., and H. Dragert (2003), Episodic tremor and slip on the Cascadia subduction zone:
366 The chatter of silent slip, *Science*, *300*, 1942–1943.
- 367 Rowe, C. D., J. C. Moore, F. Remitti, and the IODP Expedition 343/343T Scientists (2013),
368 The thickness of subduction plate boundary faults from the seafloor into the
369 seismogenic zone, *Geology*, *41*, 991–994.
- 370 Saffer, D. M., and L. M. Wallace (2015), The frictional, hydrological, metamorphic and
371 thermal habitat of shallow slow earthquakes, *Nat. Geosci.*, *8*, 594–600.
- 372 Schwartz, S. Y., and J. M. Rokosky (2007), Slow slip events and seismic tremor at
373 circum-pacific subduction zones, *Rev. Geophys.*, *45*, RG3004.
- 374 Secor, D. T. (1965), Role of fluid pressure in jointing, *Am. J. Sci.*, *263*, 633–646.

- 375 Shelly, D. R., G. C. Beroza, and S. Ide (2007), Non-volcanic tremor and low-frequency
376 earthquakes swarms, *Nature*, 446, 305–307.
- 377 Sibson, R. H. (2017), Tensile overpressure compartments on low-angle thrust faults, *Earth*
378 *Planets Space*, 69, 113.
- 379 Skarbek, R. M., A. W. Rempel, and D. A. Schmidt (2012), Geologic heterogeneity can
380 produce aseismic slip transients, *Geophys. Res. Lett.*, 39, L21306.
- 381 Ujiie, K. (2002), Evolution and kinematics of an ancient décollement zone, mélange in the
382 Shimanto accretionary complex of Okinawa Island, Ryukyu Arc, *J. Struct. Geol.*, 24,
383 937–952.
- 384 Ujiie, K., and G. Kimura (2014), Earthquake faulting in subduction zones: Insights from fault
385 rocks in accretionary prisms, *Prog Earth Planet. Sci*, 1, 1–30,
386 doi:10.1186/2197-4284-1-7.
- 387 Ujiie, K., H. Yamaguchi, A. Sakaguchi, and S. Toh (2007), Pseudotachylytes in an ancient
388 accretionary complex and implications for melt lubrication during subduction zone
389 earthquakes, *J. Struct. Geol.*, 29, 599–613.
- 390 Vrolijk, P. (1987), Tectonically driven fluid flow in the Kodiak accretionary complex, Alaska,
391 *Geology*, 15, 466–469.
- 392 Wallace, L. M., et al. (2016), Slow slip near the trench at the Hikurangi subduction zone, New
393 Zealand, *Science*, 352, 701–704.
- 394 Whittaker, J. M., et al. (2007), Major Australian-Antarctic plate reorganization at
395 Hawaiian-Emperor bend time, *Science*, 318, 83–86.

396 Yamashita, Y., et al. (2015), Migrating tremor off southern Kyushu as evidence for slow slip
397 of a shallow subduction interface, *Science*, 348, 676–679.
398

Figure 1. The Makimine mélange in the Shimanto accretionary complex. (a) Distribution of the Shimanto accretionary complex in southwest Japan. (b) Geological map of the Makimine mélange along the east coast of Kyushu. The location of the map is shown in Fig. 1a. (c) Stretching lineations developed on the surface of mélange foliation. The pencil is parallel to NNW-SSE oriented stretching lineations. The brighter bands represent intersection between foliation and kink bands. (d) Lower hemisphere equal-area stereoplots showing orientation of stretching lineations in the mélange.

Figure 2. Representative deformation in subduction mélange. Half arrows indicate sense of shear. FPEV, Foliation-parallel extension veins. (a) Macroscopic appearance of a shear vein and FPEV along the strike. (b) Slickenfibers and step (black arrow) developed on the surface of shear vein, showing thrust sense of shear. (c) Microscopic appearance of a shear vein cut parallel to slickenfibers and perpendicular to the shear surface under cross-polarized light, showing repeated episodes of cracking and sealing. The near-parallelism between phyllosilicate inclusion bands (black arrow) and the vein margin indicates that the shear vein open at a high angle to the vein margin, representing a hybrid extensional-shear fracture. (d) Folded phyllosilicate inclusion bands (black arrow) at dilational stepovers under plane-polarized light. The horizontal dark lines represent stylolites. (e) Macroscopic appearance of subvertical extension veins along the dip showing *en echelon* arrays. (f) Microscopic appearance of a subvertical extension vein under cross-polarized light. (g) Macroscopic appearance of a viscous shear zone along the dip showing thrust sense of shear. (h) Microscopic

appearance of a viscous shear zone under plane-polarized light, showing the development of asymmetric pressure solution fabric cut by subhorizontal extension veins.

Figure 3. Low-angle thrust faulting at a very low angle to σ_1 under tensile overpressure.

(a) Lower hemisphere equal-area stereoplots showing orientation of slickenfiber shear veins, *mélange* foliation, and average orientations of slickenfiber shear veins and *mélange* foliation in the vein concentration zone in the lower thrust sheet. (b) Schematic of geometrical relation between shear veins and foliation-parallel extension veins in a compressional regime with $\sigma_3 = \sigma_v$. (c) Mohr diagram showing conditions of a hybrid extensional-shear fracture at a very low angle to σ_1 . τ , shear stress; σ_n' , effective normal stress. (d) Schematic of fault-fracture meshes developed along the subduction plate boundary.

Figure 4. Sealing time for the width (w) of inclusion bands in quart-filled shear veins.

(a) At depth of 10 km and temperature of 300 °C. (b) At depth of 15 km and temperature of 330 °C.

Figure 1.

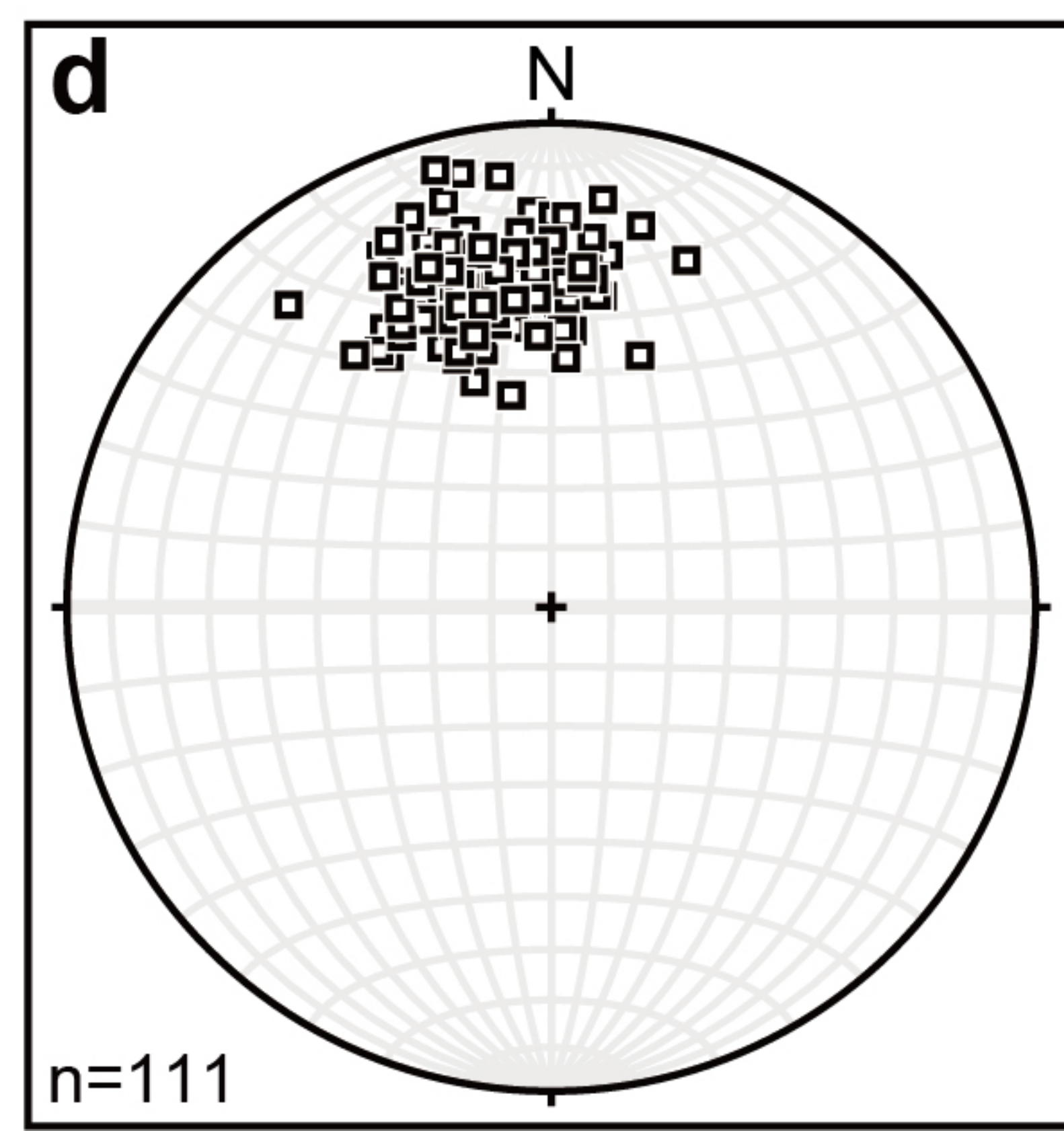
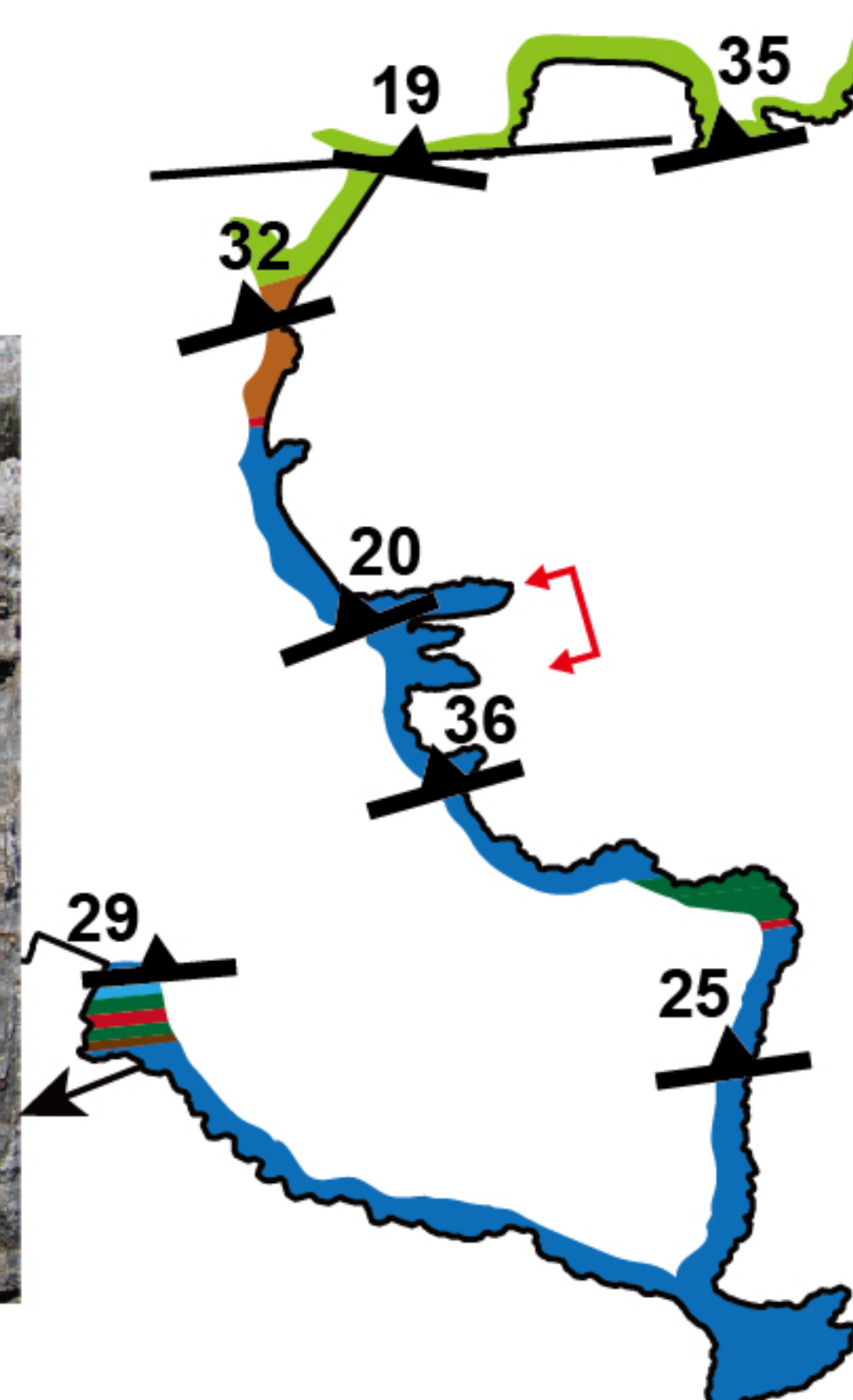
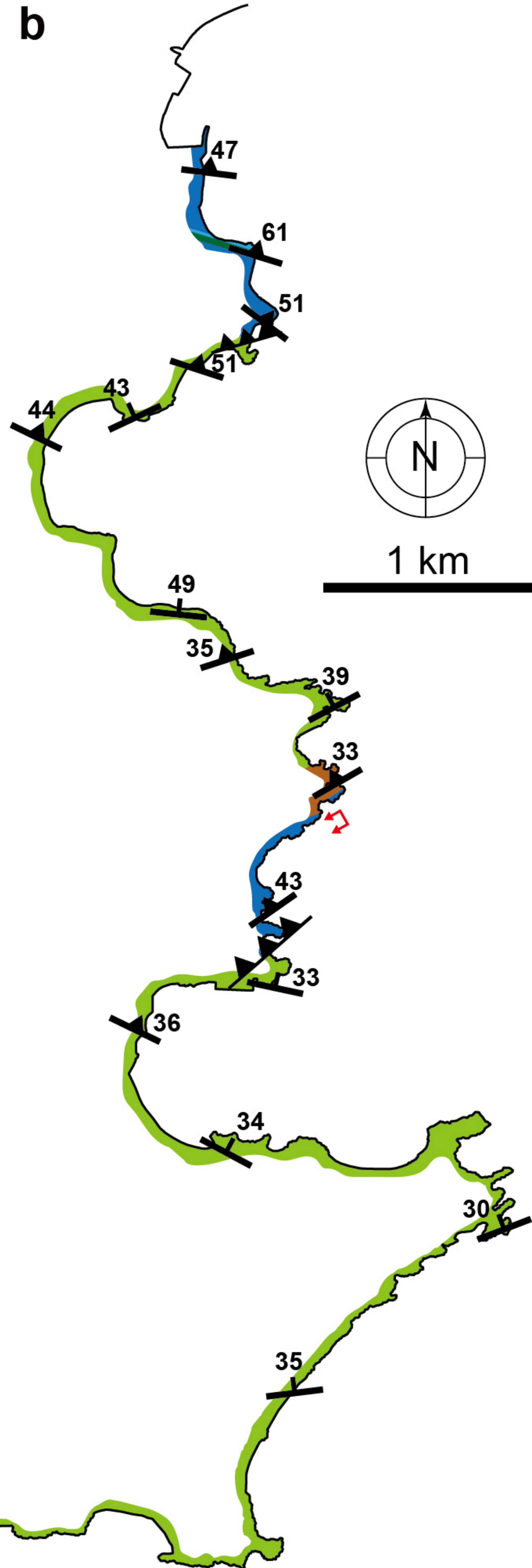
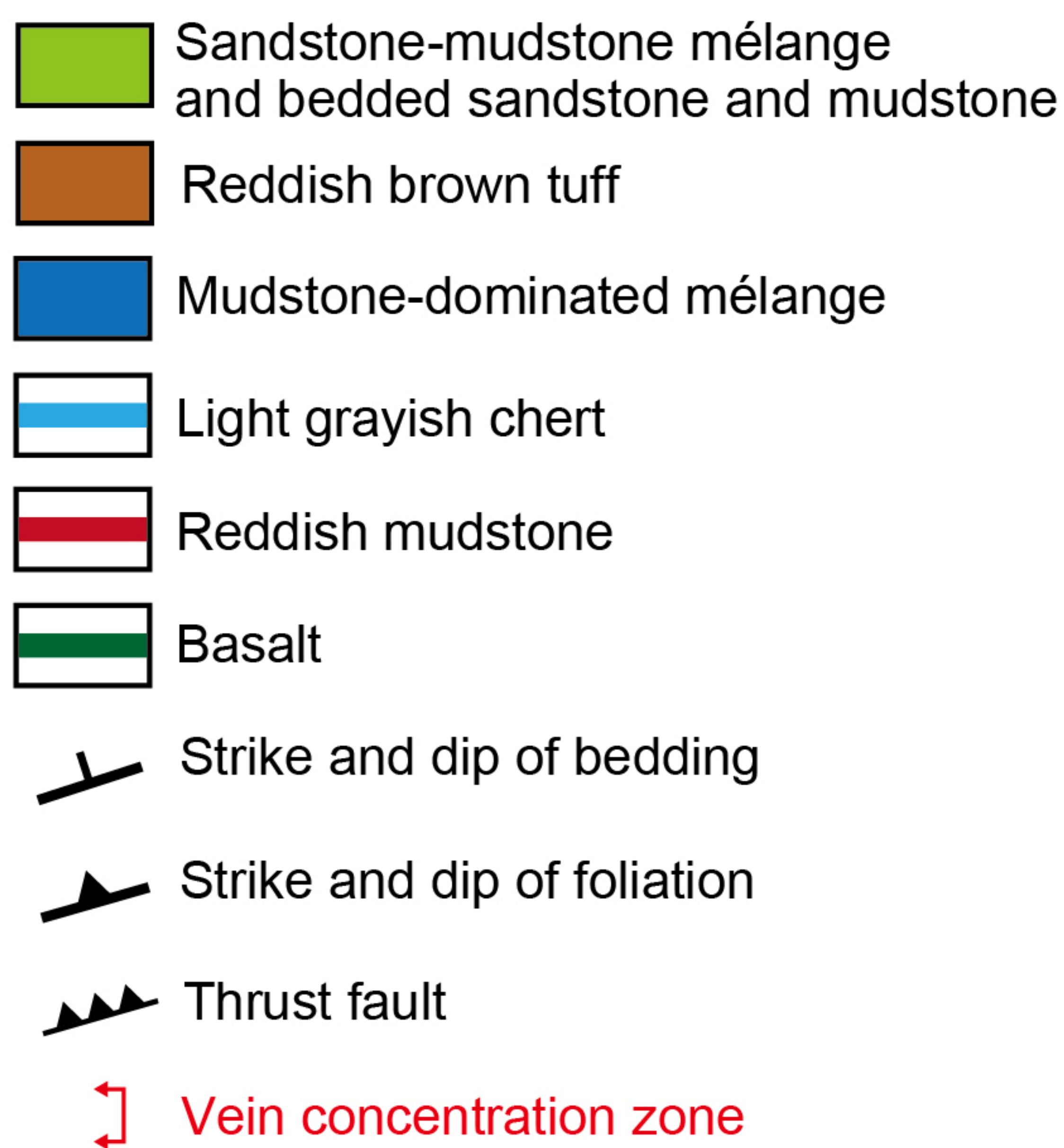
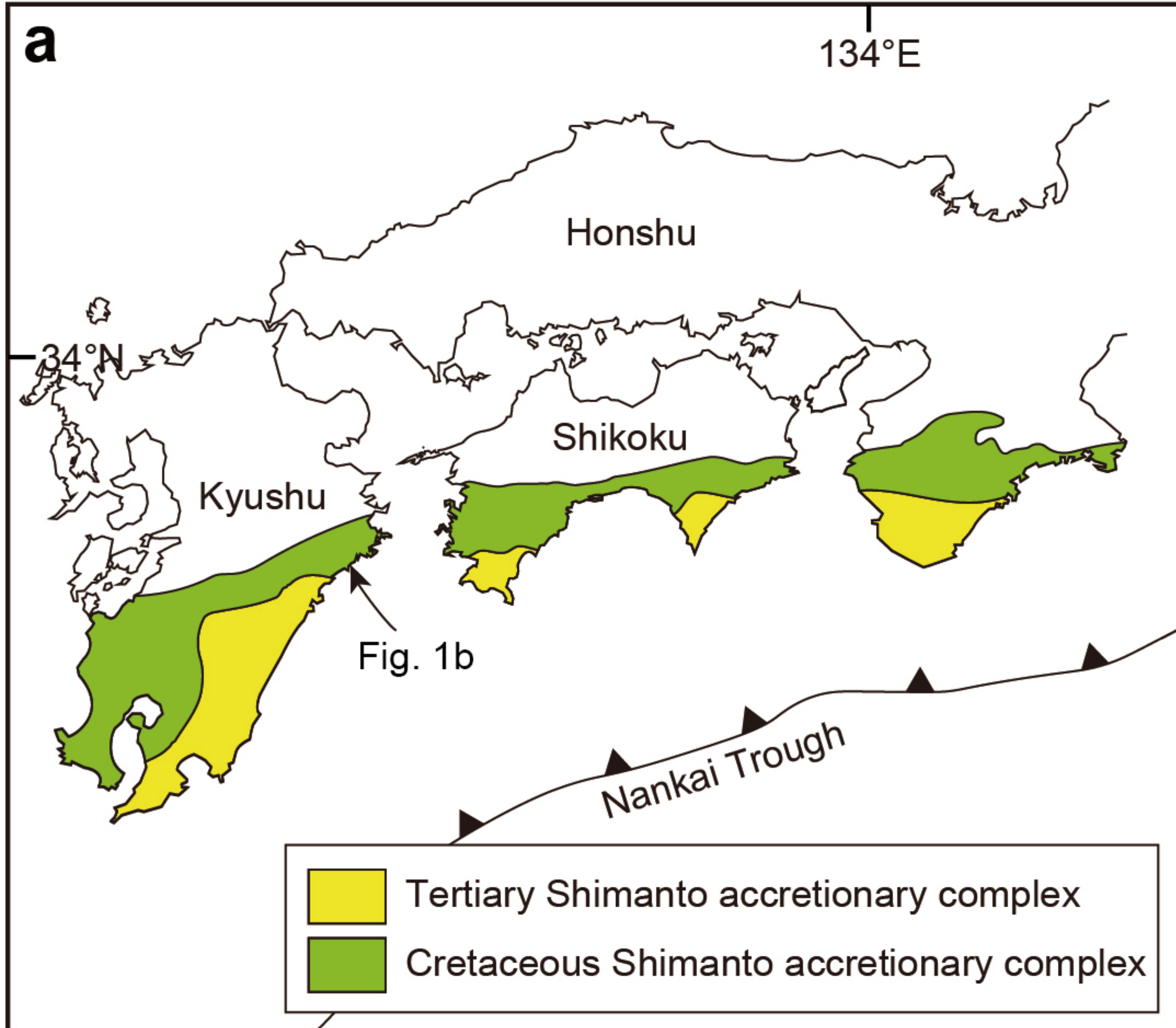


Figure 2.

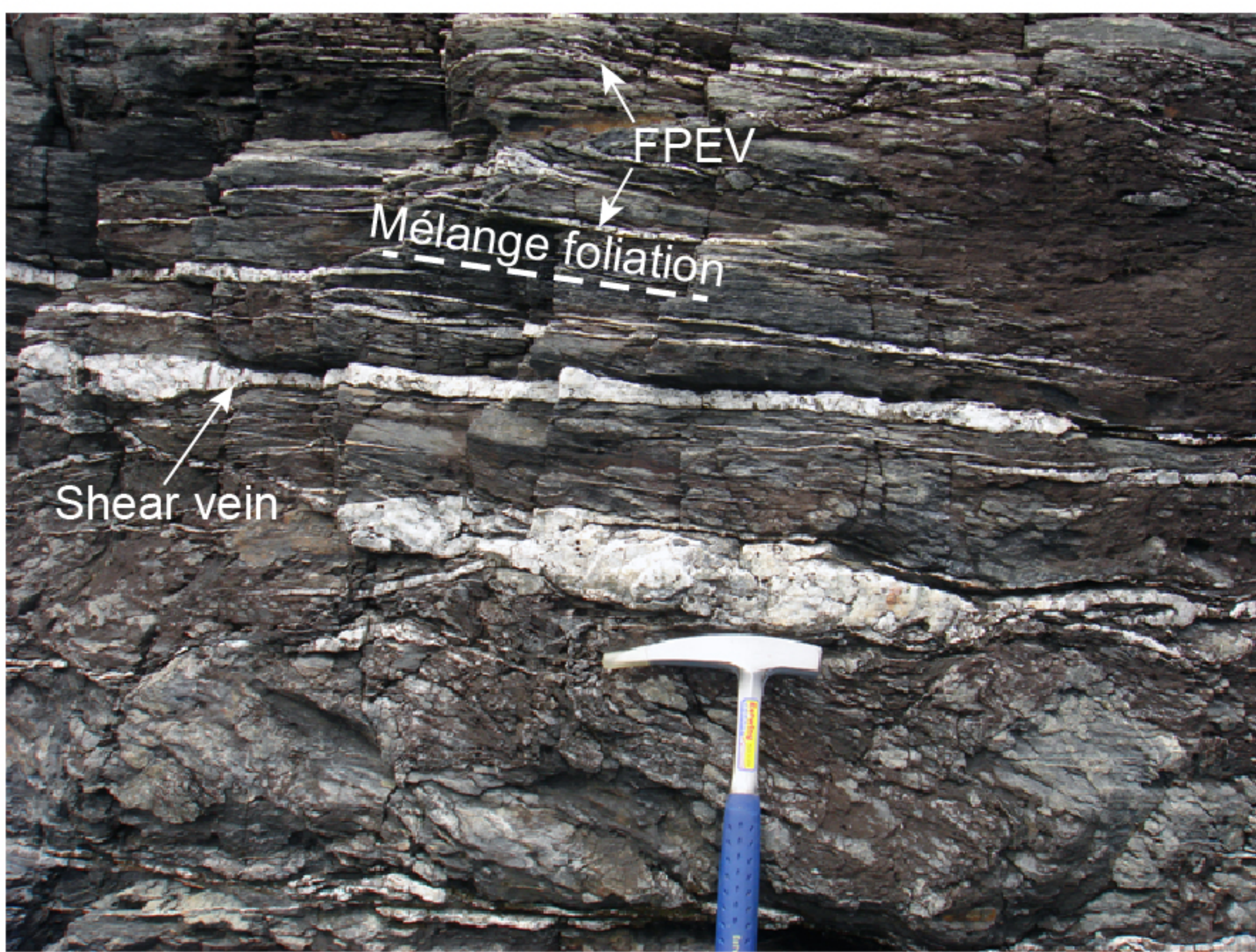
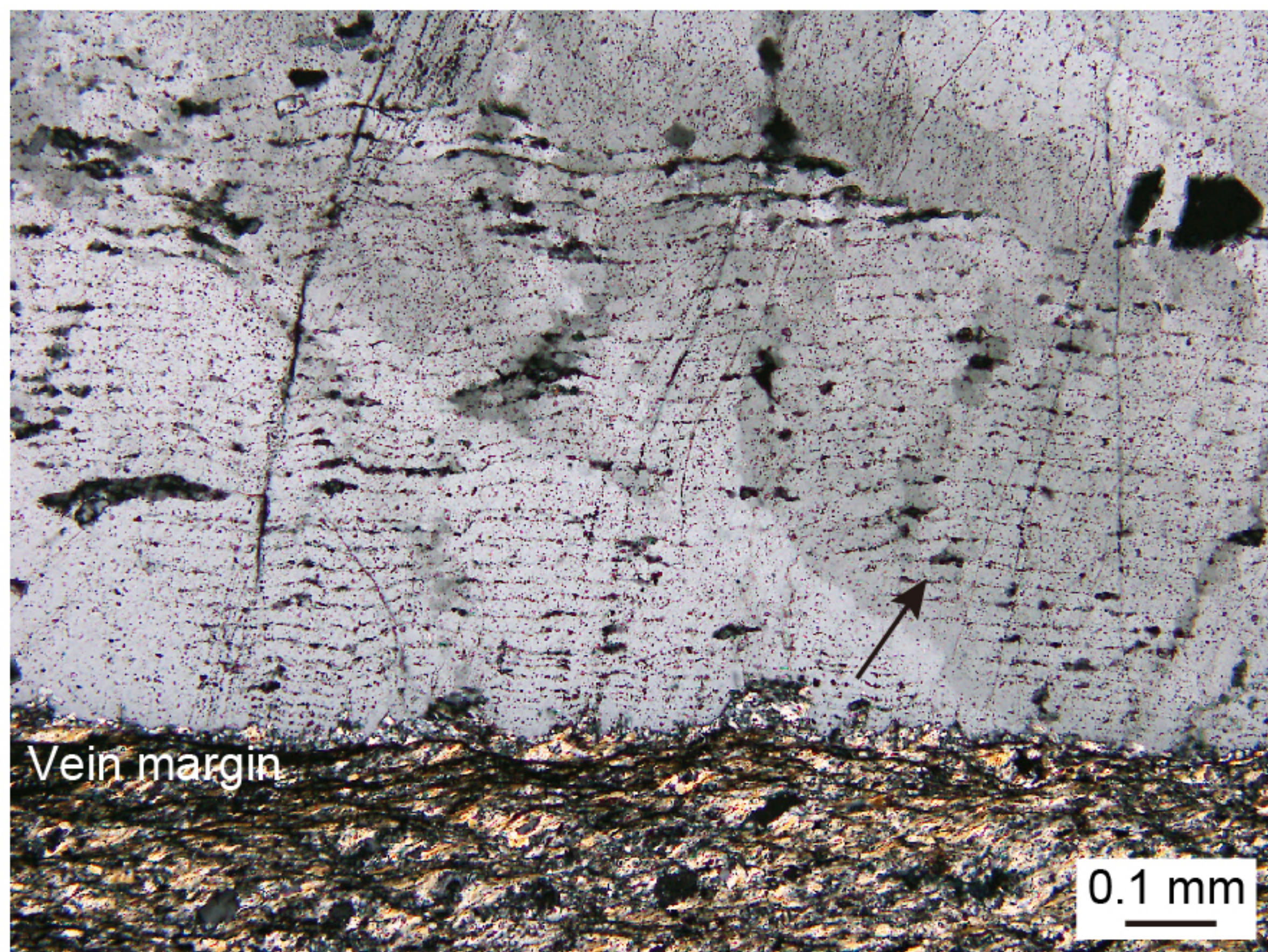
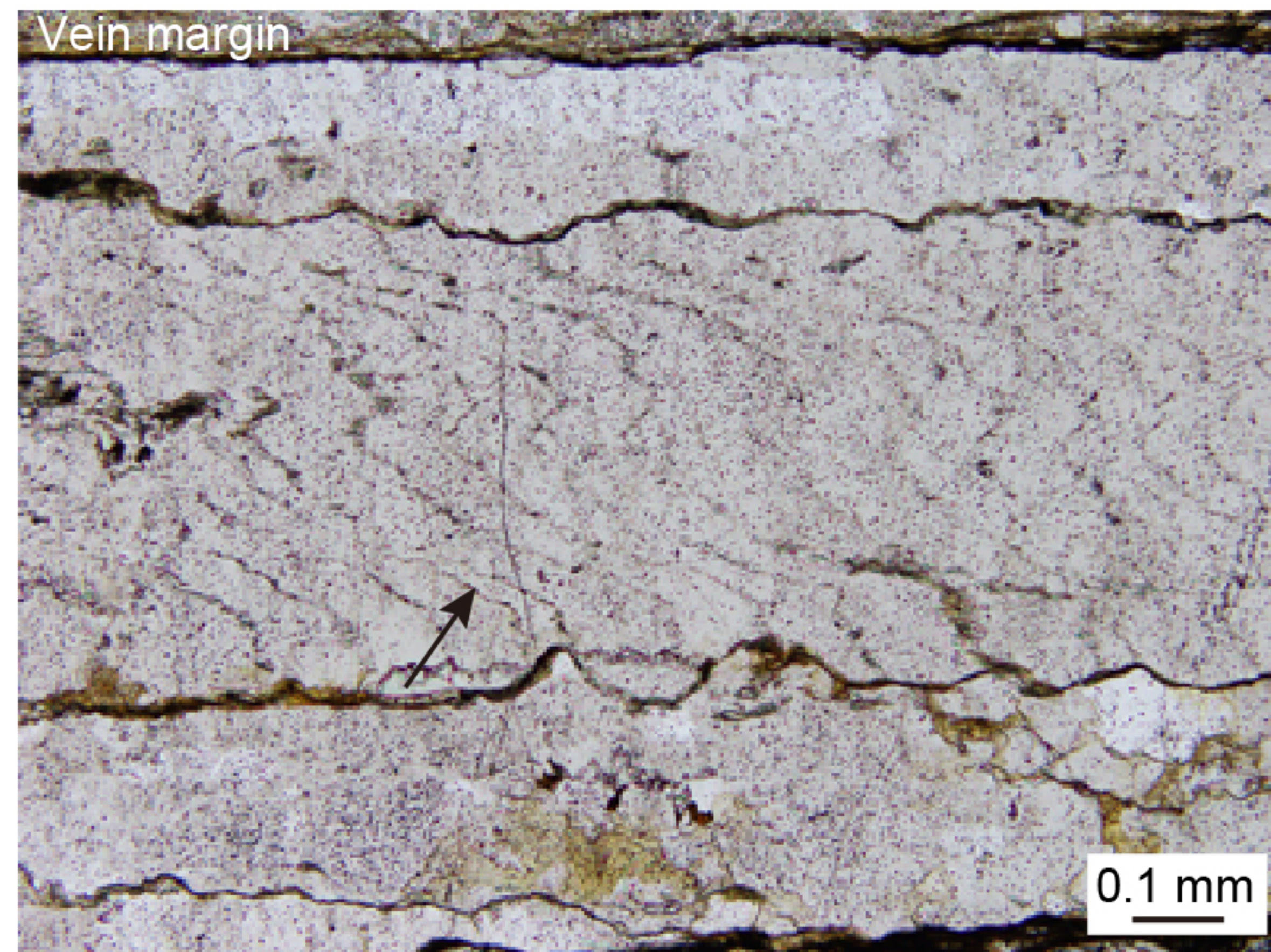
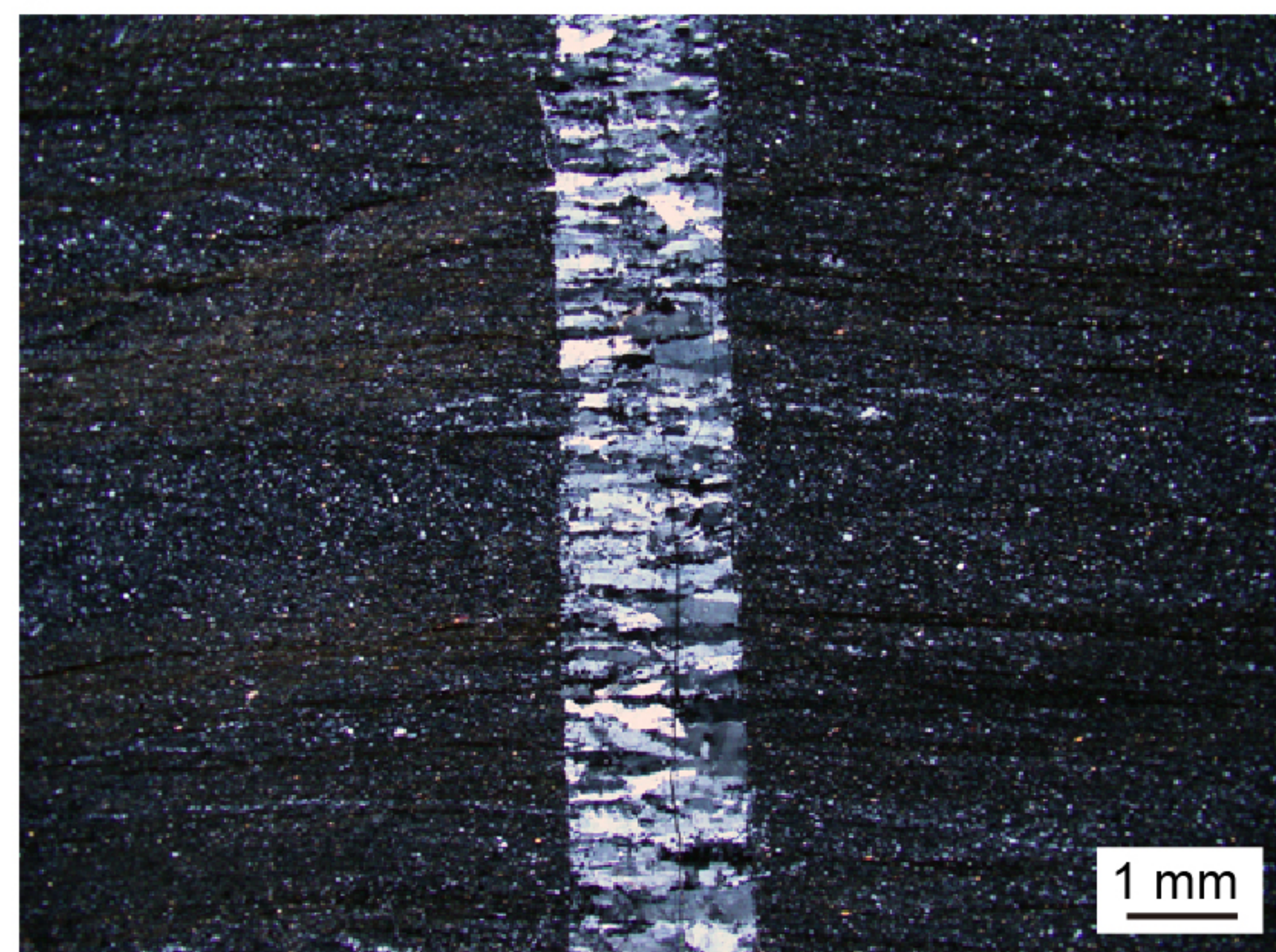
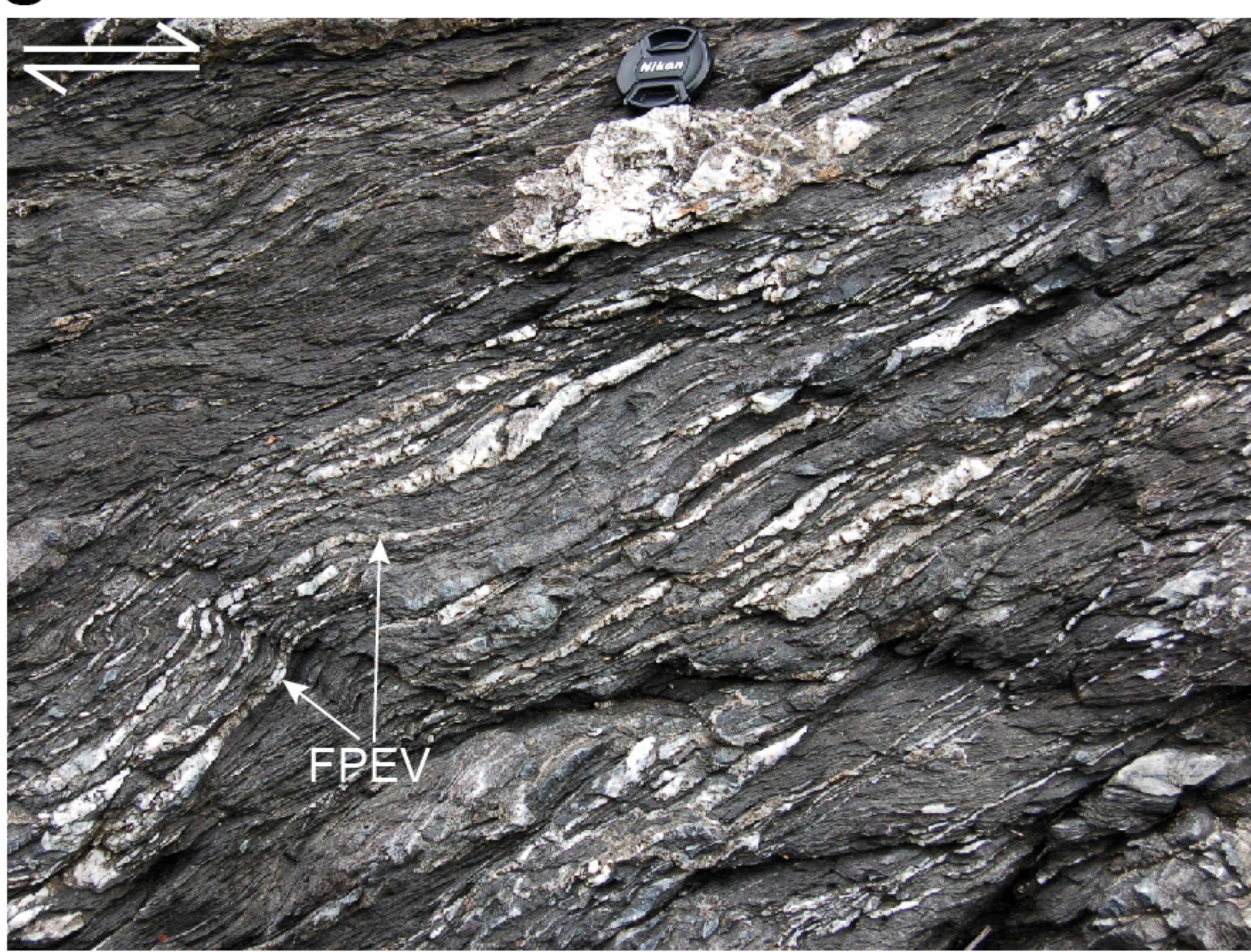
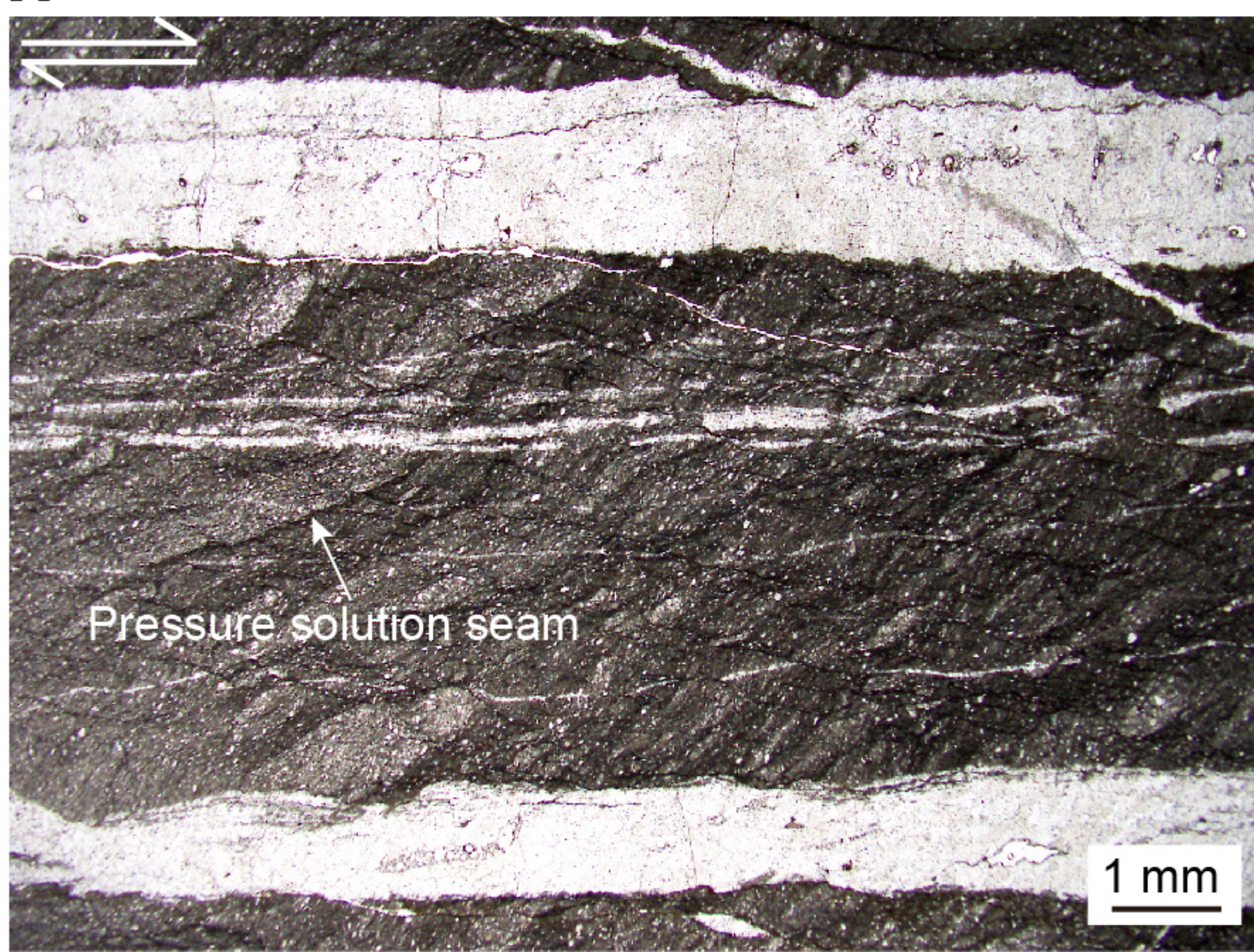
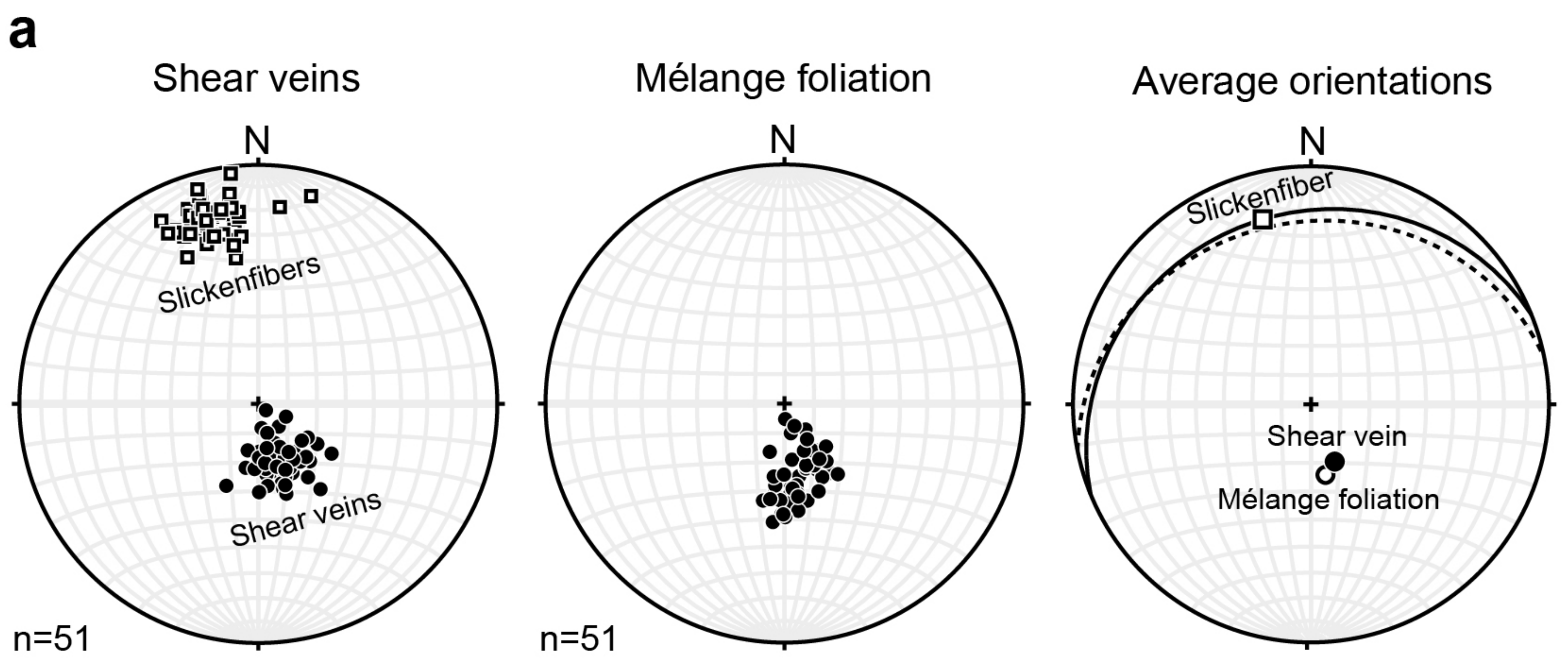
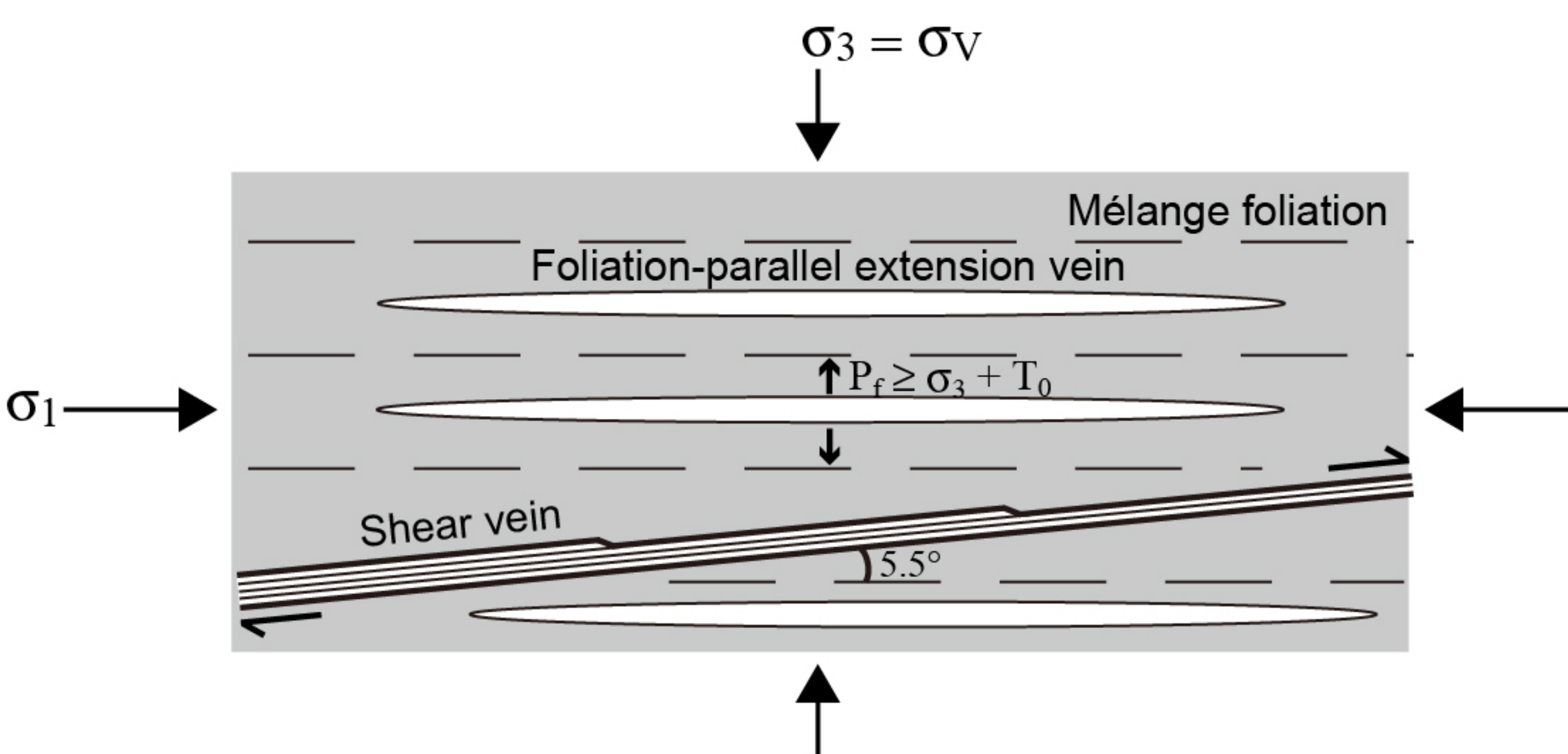
a**b****c****d****e****f****g****h**

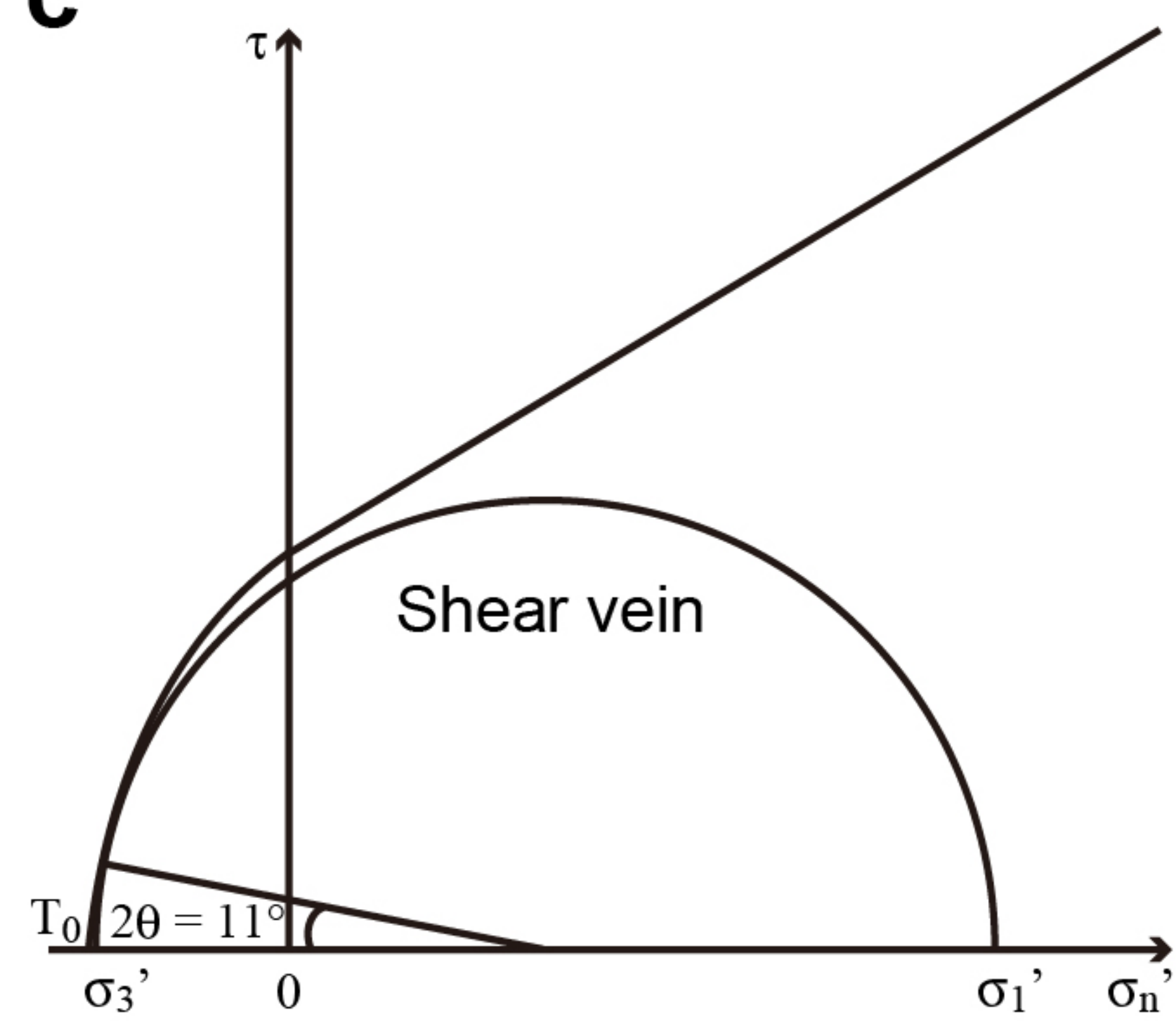
Figure 3.



b



c



d

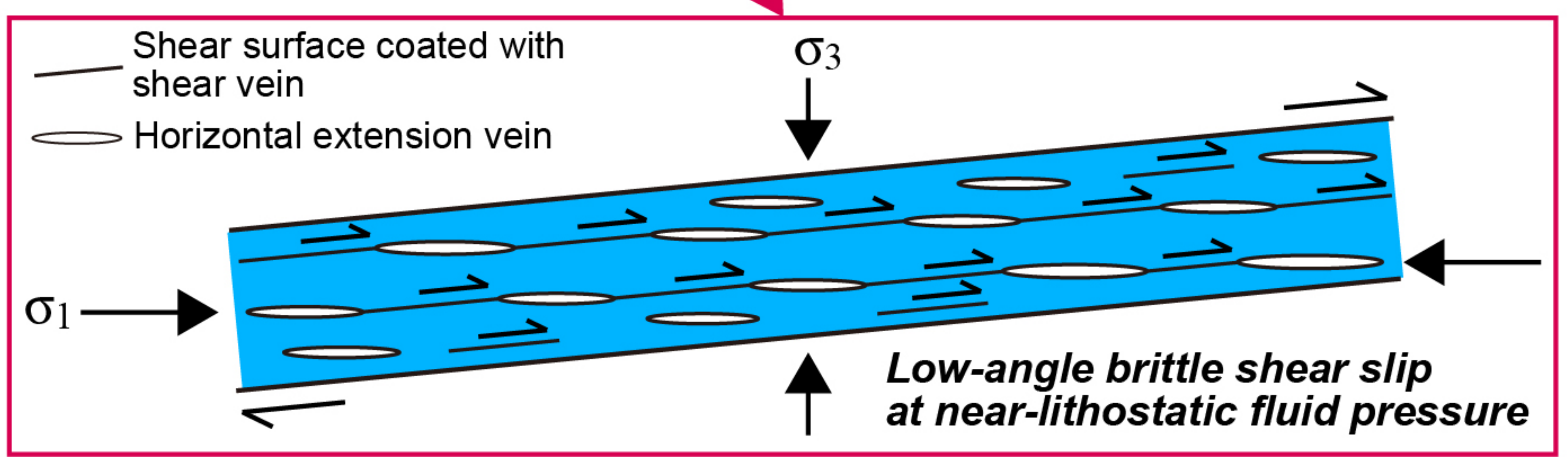
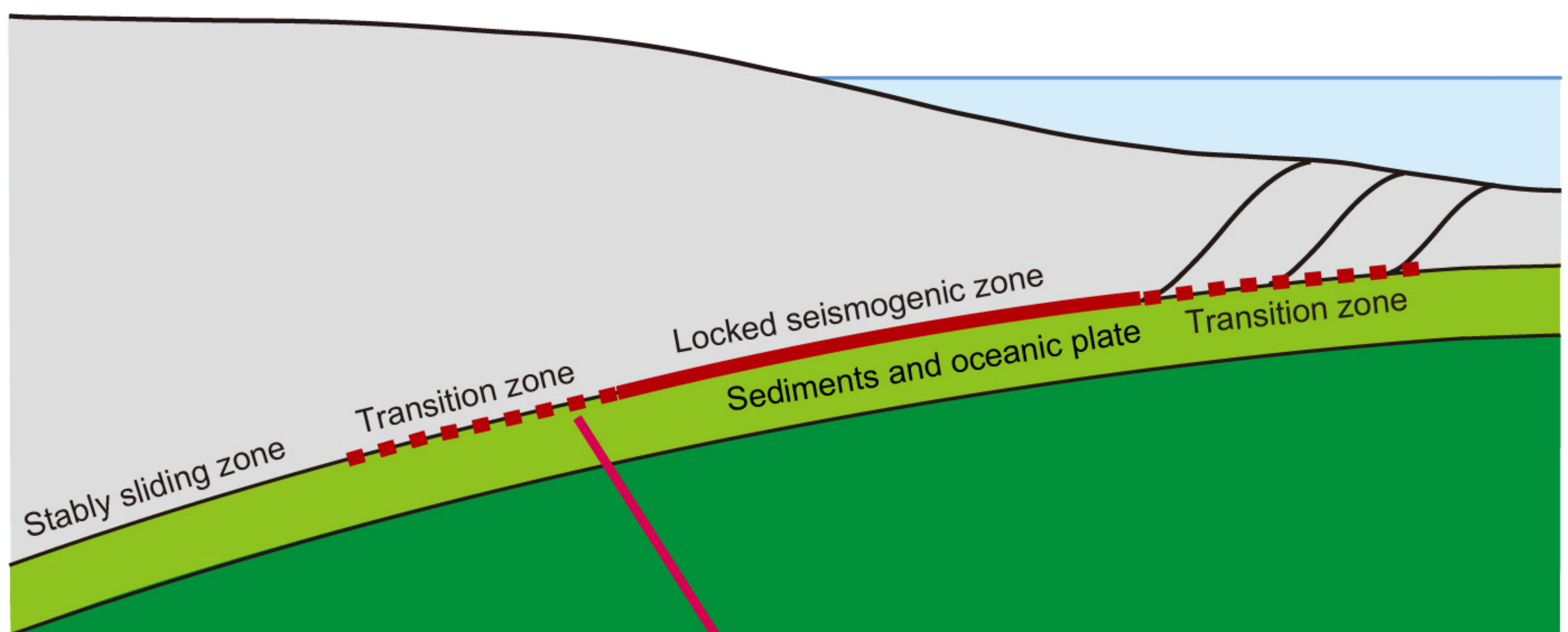
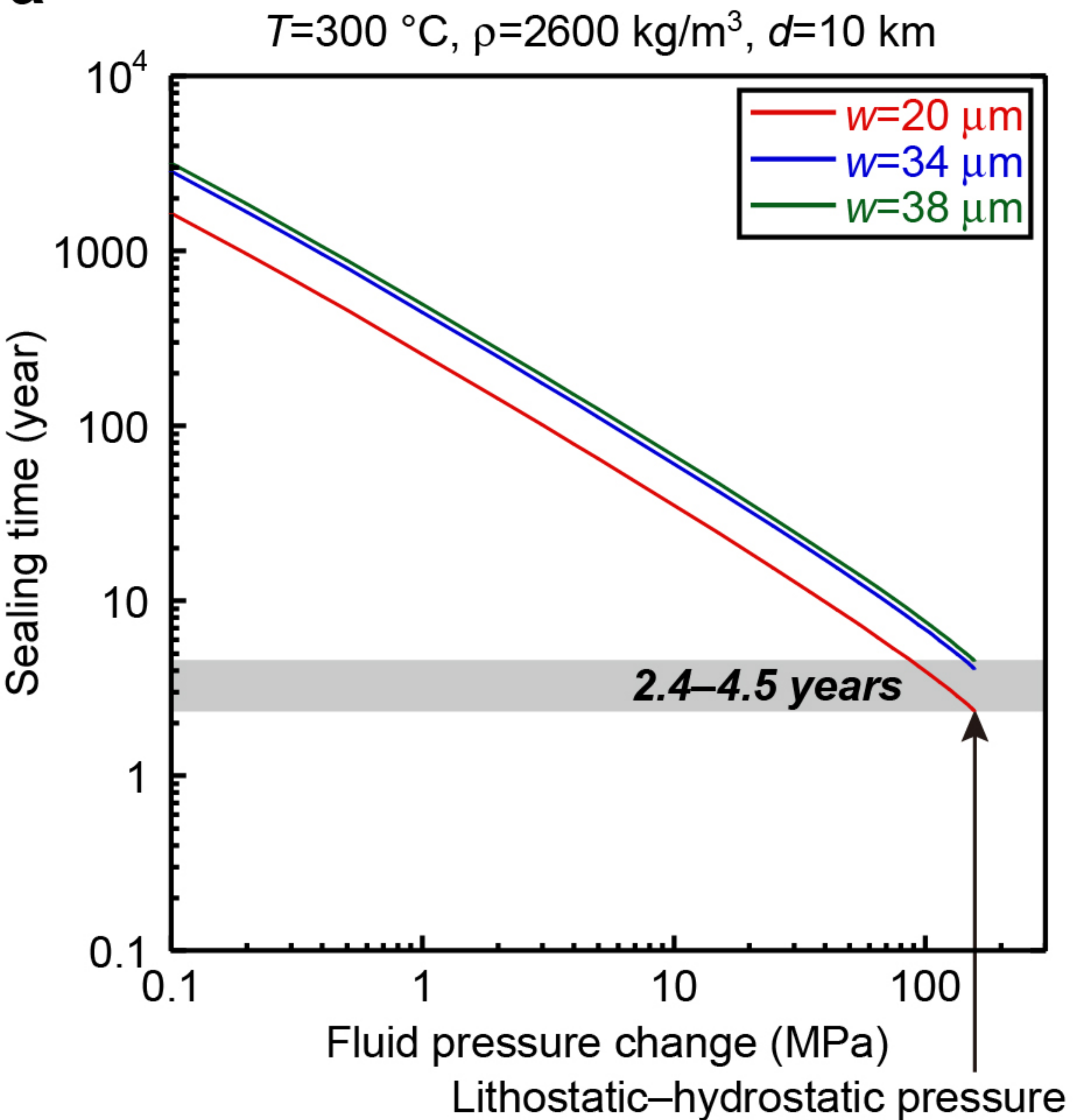


Figure 4.

a**b**